



Universiteit
Leiden
The Netherlands

Conductance and gating effects at sputtered oxide interfaces

Yin, C.

Citation

Yin, C. (2019, July 3). *Conductance and gating effects at sputtered oxide interfaces*. *Casimir PhD Series*. Retrieved from <https://hdl.handle.net/1887/74527>

Version: Not Applicable (or Unknown)

License: [Leiden University Non-exclusive license](#)

Downloaded from: <https://hdl.handle.net/1887/74527>

Note: To cite this publication please use the final published version (if applicable).

Cover Page



Universiteit Leiden



The handle <http://hdl.handle.net/1887/74527> holds various files of this Leiden University dissertation.

Author: Yin, C.

Title: Conductance and gating effects at sputtered oxide interfaces

Issue Date: 2019-07-03

A

Self-consistent Schrödinger-Poisson calculation

A.1. Introduction

The self-consistent Schrödinger-Poisson (S-P) model was first used by F. Stern to study energy levels, populations, and charge distributions in n -type inversion layers on p -type Si in 1972 [133]. It has also been used by several groups to provide valuable insights into experimental results in $\text{LaAlO}_3/\text{SrTiO}_3$ heterostructures [89, 90, 128, 132, 135].

In the S-P model, quantum effects are taken into account in the effective mass approximation, and the envelope wave function is assumed to vanish at the surface [133]. Compared to Si inversion layers, calculations for the $\text{LaAlO}_3/\text{SrTiO}_3$ interface are more complicated, which is due to the anisotropic effective mass of the Ti $3d$ orbitals and the field-dependent permittivity of the SrTiO_3 substrate [62, 91].

A.1.1. Anisotropic effective mass of Ti $3d$ orbitals

The LaAlO_3 film is grown on a SrTiO_3 (001) substrate, and the S-P calculation is performed along the growth direction, *i.e.* the z direction. The effective masses of the d_{xy} and $d_{xz,yz}$ subbands are anisotropic. We take the masses of the various bands as

$$\begin{aligned} m_{xy}^{x,y} &= m_l, & m_{xy}^z &= m_h; \\ m_{xz}^{x,z} &= m_l, & m_{xz}^y &= m_h; \\ m_{yz}^{y,z} &= m_l, & m_{yz}^x &= m_h, \end{aligned} \quad (\text{A.1})$$

where $m_l = 0.7m_e$ and $m_h = 14m_e$ [89, 124, 134], with m_e being the mass of a free electron.

A.1.2. Permittivity of SrTiO_3

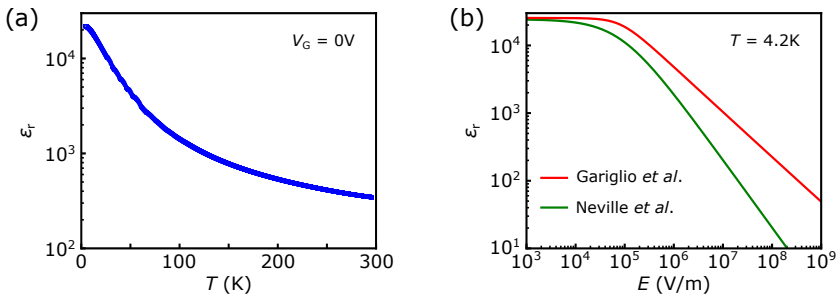


Figure A.1: (a) Temperature dependence of the permittivity (ϵ_r) of SrTiO_3 without gate voltage applied. Image adapted from Ref. [62]. (b) Electric-field dependence of ϵ_r at 4.2 K from two empirical expressions [123, 132].

SrTiO_3 single crystal has a temperature-dependent permittivity (ϵ_r) as shown in Fig. A.1(a), which reaches >20000 at low temperature. However, ϵ_r decreases when an electric

field (E) is applied to the material. So far, the field dependence of ϵ_r is still described by empirical expressions. Here, we discuss two widely used expressions. The first one was reported by Neville *et al.* [123]:

$$\epsilon_r(E) = \frac{1}{A(T) + B(T)|E|}, \quad (\text{A.2})$$

where $A(T)$ is the inverse zero-field permittivity as a function of temperature, and $B(T)$ is the field-dependent part as a function of temperature. At 4.2 K, $A = 4.097 \times 10^{-5}$ and $B = 4.907 \times 10^{-10}$ m/V for the (001) direction. The second one was reported by Gariglio *et al.* [132]:

$$\epsilon_r(E) = 1 + \frac{B}{[1 + (E/E_0)^2]^{1/3}}, \quad (\text{A.3})$$

where $B = 25462$, and $E_0 = 82213$ V/m. It can be seen from Fig. A.1(b) that the two curves overlap well in low fields but differ a lot in high fields. In LaAlO₃/SrTiO₃ heterostructures, the typical electric field at the interface is on the order of 10^7 V/m. Therefore, the two expressions can lead to very different results. We use Eq. (A.3) in our calculation.

A.2. Self-consistent Schrödinger-Poisson calculation

The S-P model involves the Schrödinger equation

$$\left(-\frac{\hbar^2}{2m_\alpha^z} \frac{d^2}{dz^2} + eV(z)\right)\psi_{n\alpha}(z) = \epsilon_{n\alpha}\psi_{n\alpha}(z), \quad n = 1, 2, 3, \dots, \quad (\text{A.4})$$

and the Poisson equation

$$-\frac{d}{dz}\left(\epsilon_0\epsilon_r(E(z))\frac{d}{dz}V(z)\right) = \rho_{3D}(z), \quad (\text{A.5})$$

where $\alpha = xy, xz, yz$ labels the Ti t_{2g} orbitals (d_{xy}, d_{xz}, d_{yz}), $V(z)$ is the confining potential, $\psi_{n\alpha}(z)$ and $\epsilon_{n\alpha}$ are normalized wave function and eigen value of the n th sub-band of the α orbital, respectively, ϵ_0 is the vacuum permittivity, and $\rho_{3D}(z)$ is the three-dimensional (3D) charge distribution.

At the LaAlO₃/SrTiO₃ interface, electrostatic confinement is described by the confining potential $V(z)$, which can be calculated by the Poisson equation. For a given charge distribution and electrostatic boundary conditions, $V(z)$ is uniquely defined. On the other hand, for a given $V(z)$, the distribution of mobile electrons is determined by the population of bound states in $V(z)$, which can be calculated by the Schrödinger equation. Therefore, the coupling between these two equations could enable a self-consistent calculation of $V(z)$. A schematic of the self-consistent S-P calculation is shown in Fig. A.2.

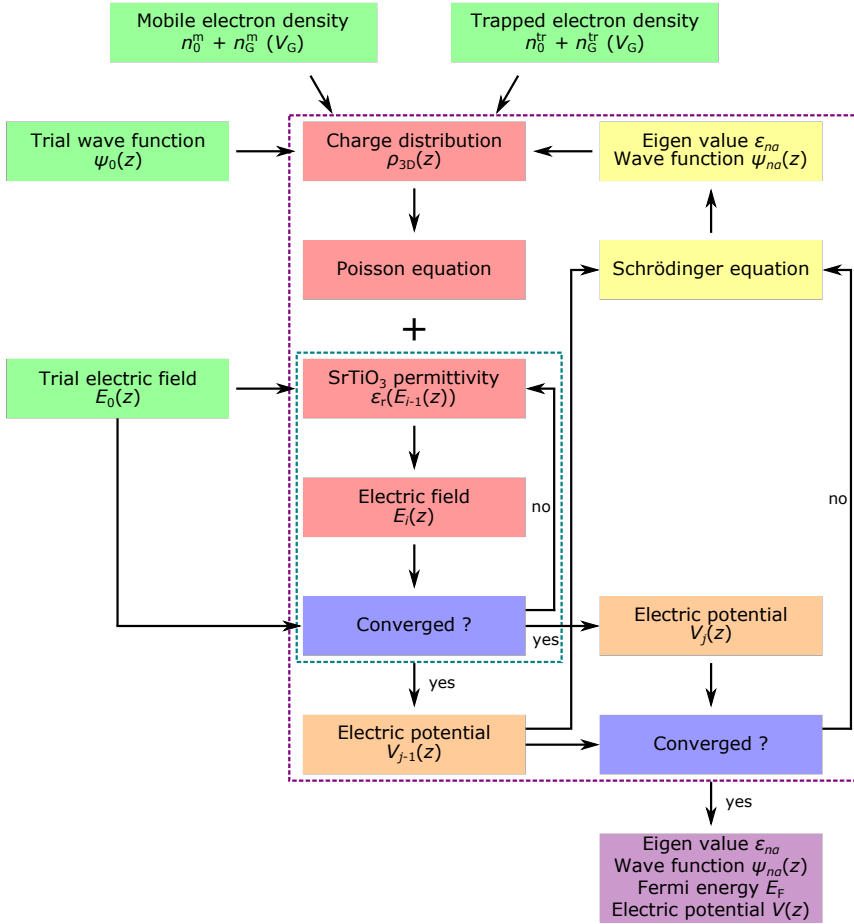


Figure A.2: Schematic of the Schrödinger-Poisson calculation, which contains two self-consistent loops. The first loop (dotted teal box) is for calculating the electric field $E(z)$ and the second loop (dotted purple box) for the electric potential $V(z)$.

A.2.1. Input parameters

Input parameters of the S-P calculation include the initial mobile electron density n_0^m , the initial trapped electron density n_0^{tr} , the gate-induced mobile electron density $n_G^m(V_G)$, the gate-induced trapped electron density $n_G^{\text{tr}}(V_G)$, a trial wave function $\psi_0(z)$, and a trial electric field $E_0(z)$. Now we discuss them one by one.

Initial mobile and trapped electron density

Initial mobile electron density n_0^m is the sheet carrier density of the virgin state, which is obtained from magnetotransport measurement. In our sample, $n_0^m = 1.41 \times 10^{13} \text{ cm}^{-2}$. Initial trapped electron density n_0^{tr} can only be obtained from trial and error until the calculated results cover the experimental results. In our case, $n_0^{\text{tr}} = 6.4 \times 10^{13} \text{ cm}^{-2}$. We take $z \geq 0$ to be SrTiO₃ and $z < 0$ to be LaAlO₃. The positive charge density is $n_0^m + n_0^{\text{tr}}$ on the LaAlO₃ side as the boundary condition, which keeps an overall charge neutrality.

Gate-induced mobile and trapped electron density

In back-gating experiment, the total amount of electrons $n_G^{\text{tot}}(V_G)$ induced by the gate voltage (V_G) can be calculated using a parallel plate capacitor model [130, 131]:

$$n_G^{\text{tot}}(V_G) = \int_{V_1}^{V_2} \frac{\epsilon_0}{ed_{\text{STO}}} \epsilon_r(V_G) dV_G, \quad (\text{A.6})$$

where $d_{\text{STO}} = 0.5 \text{ mm}$ is the thickness of the SrTiO₃ substrate, and $E = V_G/d_{\text{STO}}$. It should be noted that the electric field E here is considered to be position independent. The reason is that E only changes significantly at the interface within about 20 nm and is constant in the SrTiO₃ bulk. As discussed in Chapter 4, the gate-induced trapped electron density $n_G^{\text{tr}}(V_G)$ can only be obtained from experimental results. In our sample,

$$n_G^{\text{tr}}(V_G) = N(1 - e^{-\frac{V_G}{400}}), \quad (\text{A.7})$$

where $N = 6.2 \times 10^{13} \text{ cm}^{-2}$. Therefore, the gate-induced mobile electron density

$$n_G^m(V_G) = n_G^{\text{tot}}(V_G) - n_G^{\text{tr}}(V_G). \quad (\text{A.8})$$

Trial wave function and trial electric field

A trial wave function ($\psi_0(z)$) gives a first guess of the mobile charge distribution. We use the Fang-Howard variational wave function, which gives a good approximation for the ground state in the z direction [131]

$$\psi_0(z) = \sqrt{\frac{b^3}{2}} z e^{-\frac{bz}{2}}, \quad (\text{A.9})$$

where b is the variational parameter

$$b = \left(\frac{33\pi}{2} (n_0^m + n_G^m(V_G)) a_B^2 \right)^{\frac{1}{3}} \frac{1}{a_B}, \quad (\text{A.10})$$

where a_B is the Bohr radius

$$a_B = \frac{4\pi\epsilon_r\epsilon_0\hbar^2}{m^*e^2}. \quad (\text{A.11})$$

It should be noted that the actual input values for Eq. (A.11) do not affect the final results. We take $\epsilon_r = 1$ and $m^* = m_e$.

A trial electric field ($E_0(z)$) can be any reasonable value and we take $E_0(z) = 1000 \text{ V/m}$.

A.2.2. Self-consistent calculation

First, we calculate the 3D charge distribution $\rho_{3D}(z)$, which is the sum of the distribution of mobile and trapped electrons,

$$\rho_{3D}(z) = \rho_{3D}^m(z) + \rho_{3D}^{\text{tr}}(z). \quad (\text{A.12})$$

The mobile charge distribution is given by

$$\rho_{3D}^m(z) = -e(n_0^m + n_G^m(V_G)) |\psi_0(z)|^2. \quad (\text{A.13})$$

The trapped charge distribution should also be obtained from trial and error. In our sample,

$$\rho_{3D}^{\text{tr}}(z) = \begin{cases} 0 & \text{for } z < 0 \\ -e \frac{n_0^{\text{tr}} + n_G^{\text{tr}}(V_G)}{\lambda} e^{-\frac{z}{\lambda}} & \text{for } z \geq 0 \end{cases} \quad (\text{A.14})$$

where $\lambda = 50 \text{ nm}$.

Integration of Eq. (A.5) along the z direction gives

$$-\epsilon_0\epsilon_r(E(z)) \frac{d}{dz} V(z) = -\epsilon_0\epsilon_r(E(z)) E(z) = \int_0^L \rho_{3D}(z) dz, \quad (\text{A.15})$$

where the integration range is from 0 to $L = 100 \text{ nm}$, which is divided into 2000 equal sections.

Now we enter the first self-consistent loop for calculating $E(z)$ as shown in Fig. A.2. The convergence is checked by

$$\eta = \frac{1}{L} \int_0^L \left(\frac{E_i(z) - E_{i-1}(z)}{E_i(z)} \right)^2 dz. \quad (\text{A.16})$$

If η is large than the error tolerance ϵ_p (set to 10^{-5}), a new electric field ($E'_i(z)$) is calculated by the over relaxation method in order to get a faster convergence

$$E'_i(z) = \zeta E_{i-1}(z) + (1 - \zeta) E_i(z), \quad (\text{A.17})$$

where $\zeta = 0.3$. If η is smaller than ϵ_p , the calculation is converged. Integration of $E_i(z)$ along the z direction gives the electric potential $V_{j-1}(z)$.

Next, $V_{j-1}(z)$ is injected into Eq. (A.4). The outcome of solving the Schrödinger equation is the eigen values ($\epsilon_{n\alpha}$) and the normalized wave functions ($\psi_{n\alpha}(z)$) of the subbands of different t_{2g} orbitals. We can calculate the mobile charge distribution again with $\epsilon_{n\alpha}$ and $\psi_{n\alpha}(z)$:

$$\rho_{3D}^m(z) = -e \sum_{n,\alpha} \Theta(E_F - \epsilon_{n\alpha}) \frac{\sqrt{m_\alpha^x m_\alpha^y}}{\pi \hbar^2} (E_F - \epsilon_{n\alpha}) |\psi_{n\alpha}(z)|^2, \quad (\text{A.18})$$

where Θ is the Heaviside step function and E_F is the Fermi energy. E_F can be obtained by numerically solving

$$n_0^m + n_G^m(V_G) = \sum_{n,\alpha} \Theta(E_F - \epsilon_{n\alpha}) \frac{\sqrt{m_\alpha^x m_\alpha^y}}{\pi \hbar^2} (E_F - \epsilon_{n\alpha}). \quad (\text{A.19})$$

A new $\rho_{3D}(z)$ is obtained by summing up Eq. (A.14) and Eq. (A.18).

Now we enter the larger self-consistent loop for calculating $V(z)$ as shown in Fig. A.2. By treating the new electric potential $V_j(z)$ and $V_{j-1}(z)$ with the same manner as shown in Eq. (A.16) and Eq. (A.17), a converged electric potential $V(z)$ can be obtained.

The subband dispersion can be calculated by

$$E_{n\alpha} = \frac{\hbar^2 k_x^2}{2m_\alpha^x} + \frac{\hbar^2 k_y^2}{2m_\alpha^y} + \epsilon_{n\alpha}, \quad (\text{A.20})$$

where k_x and k_y are the wavevector in the x and y directions, respectively.

